Baghdad Science Journal

Volume 23 | Issue 1 Article 2

1-1-2026

Green Synthesis of TiO_2 Nanoparticles via Graphene Oxide-Doped Malabar Spinach Leaf Extract for Perovskite Solar Cells

Nofrijon Sofyan
Advanced Materials Research Center, Faculty of Engineering, Universitas Indonesia, Depok 16424, Indonesia AND Department of Metallurgical and Materials Engineering, Faculty of Engineering, Universitas Indonesia, Depok 16424, Indonesia, nofrijon.sofyan@ui.ac.id

Ichsan Pandu Wicaksono
Department of Metallurgical and Materials Engineering, Faculty of Engineering, Universitas Indonesia, Depok 16424, Indonesia, ichsanpanduwicaksono@gmail.com

Fiona Angellinnov
Department of Metallurgical and Materials Engineering, Faculty of Engineering, Universitas Indonesia, Depok 16424, Indonesia, fiona.angellinnov31@ui.ac.id

Aga Ridhova
Research Center for Metallurgy, National Research and Innovation Agency, Tangerang Selatan, Banten 15314, Indonesia, aga.ridhova@brin.go.id

Akhmad Herman Yuwono
Advanced Materials Research Center, Faculty of Engineering, Universitas Indonesia, Depok 16424, Indonesia AND Department of Metallurgical and Materials Engineering, Faculty of Engineering, Universitas Indonesia, Depok 16424, Indonesia, ahyuwono@eng.ui.ac.id

DOI: https://doi.org/10.21123/2411-7986.5135

Green Synthesis of TiO_2 Nanoparticles via Graphene Oxide-Doped Malabar Spinach Leaf Extract for Perovskite Solar Cells

Authors

Nofrijon Sofyan, Ichsan Pandu Wicaksono, Fiona Angellinnov, Aga Ridhova, Akhmad Herman Yuwono, and Donanta Dhaneswara

BAGHDAD SCIENCE JOURNAL 2026;23(1):16–29

SPECIAL ISSUE ARTICLE

Green Synthesis of TiO_2 Nanoparticles via Graphene Oxide-Doped Malabar Spinach Leaf Extract for Perovskite Solar Cells

Nofrijon Sofyan [1,2,*], **Ichsan Pandu Wicaksono** [2], **Fiona Angellinnov** [2], **Aga Ridhova** [3], **Akhmad Herman Yuwono** [1,2], **Donanta Dhaneswara** [1,2]

[1] Advanced Materials Research Center, Faculty of Engineering, Universitas Indonesia, Depok 16424, Indonesia
[2] Department of Metallurgical and Materials Engineering, Faculty of Engineering, Universitas Indonesia, Depok 16424, Indonesia
[3] Research Center for Metallurgy, National Research and Innovation Agency, Tangerang Selatan, Banten 15314, Indonesia

ABSTRACT

This study investigates a green synthesis route for titanium dioxide (TiO_2) nanoparticles (NPs) using Malabar spinach (*Basella rubra*) leaf extract, with graphene oxide (GO) as a dopant, for application as an electron transport layer in perovskite solar cells (PSCs). The synthesized TiO_2 NPs were characterized using Fourier transform infrared spectroscopy (FTIR), X-ray diffraction (XRD), ultraviolet-visible diffuse reflectance spectroscopy (UV-Vis DRS), and field emission scanning electron microscopy equipped with energy dispersive X-ray spectroscopy (FESEM/EDX). XRD results confirmed the presence of a pure anatase phase with a smaller crystallite size than that of commercial TiO_2, while EDX analysis verified the successful synthesis through elemental analysis. FESEM imaging revealed a mixture of rugged and uniformly distributed nanoparticles. Optical studies showed a reduced bandgap energy (3.0400 eV) compared to commercial TiO_2 (3.2000 eV), indicating improved light absorption potential. The integration of GO suggestively enhanced photovoltaic performance, with the highest power conversion efficiency (0.2467%) observed in the sample synthesized using distilled water, leaf extract, and GO—an order of magnitude higher than commercial TiO_2 (0.0259%). However, performance varied notably with different synthesis media, suggesting that solvent-specific interactions play a critical role in determining device efficiency. These findings demonstrate the viability of eco-friendly synthesis in developing functional nanomaterials and highlight the synergistic benefits of combining plant-based reductants and GO doping. The approach offers a promising pathway toward more sustainable and cost-effective PSC technologies; however, optimizing plant extract composition and nanoparticle morphology remains essential.

Keywords: *Basella rubra*, Graphene oxide, Green synthesis, Malabar spinach, Titanium dioxide nanoparticles

Introduction

Reducing greenhouse gas (GHG) emissions is a key global priority, as energy-related emissions account for over three-quarters of total GHGs worldwide.[1] Global energy consumption has increased by one-third since 2000 and is projected to rise substantially by 2050, driven by population and economic growth.[2] In light of intensifying global warming, transitioning to cleaner energy sources—such as solar energy—has become increasingly urgent.[3] Among emerging solar technologies, perovskite solar cells (PSCs) have garnered considerable interest due to their efficiency and potential for low-cost production. These devices typically incorporate perovskite-structured compounds (ABX_3),[4] where A is an organic cation (such as methylammonium or formamidinium), B is a metal (lead or tin), and X is a

Received 23 February 2025; revised 27 June 2025; accepted 2 October 2025.
Available online 1 January 2026

* Corresponding author.
E-mail addresses: nofrijon.sofyan@ui.ac.id (N. Sofyan), ichsanpanduwicaksono@gmail.com (I. P. Wicaksono), fiona.angellinnov31@ui.ac.id (F. Angellinnov), aga.ridhova@brin.go.id (A. Ridhova), ahyuwono@eng.ui.ac.id (A. H. Yuwono), donanta.dhaneswara@ui.ac.id (D. Dhaneswara).

International Conference on Discoveries in Applied Sciences and Applied Technology (DASAT2025)
https://doi.org/10.21123/2411-7986.5135

halogen (Cl, Br, or I) that serves as the light-absorbing layer.[5,6]

In advancing solar cells, nanomaterials have proven instrumental in enhancing device performance by enabling light-trapping architectures, forming interlayer transmission bridges, and facilitating efficient charge-carrier transport pathways.[7] Among these, titanium dioxide (TiO_2) nanomaterials, particularly TiO_2 nanoparticles (NPs), are favored over their bulk counterparts due to their superior optoelectronic properties and larger surface area, which improve interfacial charge dynamics.[8,9] TiO_2 commonly serves as the electron transport layer in perovskite solar cells; however, its relatively wide bandgap energy of 3.2 eV restricts absorption to the UV spectrum, thereby limiting the utilization of visible light.[10] To address this limitation, extensive research has been devoted by many investigators to narrowing TiO_2's bandgap through techniques such as elemental doping,[11] quantum confinement effects,[12] and defect mediation strategies.[13]

Several routes are available for synthesizing TiO_2, including the conventional physical top-down method and the chemical bottom-up process, both of which form TiO_2 nanoparticles (NPs).[14,15] Some top-down conventional methods include lithography and laser ablation.[16,17] Notwithstanding their simplicity, these approaches require high energy and high initial costs. The bottom-up approaches, such as chemical vapor deposition (CVD),[18] hydrothermal,[19,20] and the conventional sol–gel method,[21,22] result in well-defined shapes and sizes, narrow size distributions of nanoparticles, and cost-effectiveness. These techniques, however, have some disadvantages, including complex chemistry and the generation of toxic chemical waste.[23] As an alternative to these conventional methods, the green synthesis approach has gained interest in nanotechnology, particularly in the synthesis of TiO_2 NPs.[24] It has emerged as a promising alternative, offering a more sustainable and cost-effective route for producing TiO_2 NPs using biological materials, such as plant extracts. Numerous plant species have been utilized by various investigators for the green synthesis of metal oxide nanoparticles, including orange peel,[25] *Terminalia catappa*,[26] *Uncaria gambir*,[27] Mangosteen,[28] *Morus nigra*,[29,] and *Citrus limon*.[30] Malabar spinach (*Basella rubra*) has been known to contain active compounds that act as stabilizing agents during the formation of nanoparticles.[31,32] None has been used for perovskite solar cells applications.

Graphene oxide (GO), known for its high electron mobility and enhanced stability, has been incorporated as a dopant in TiO_2 NPs to improve the power conversion efficiency of a dye-sensitized solar cell (DSSC).[26] However, sufficient research is still lacking in this field, presenting inconsistencies and limitations, and has not been fully explored. Additionally, while green synthesis methods aim to reduce environmental impact, challenges remain in achieving consistent particle size, morphology, and crystallinity, which are crucial for optimizing the performance of TiO_2 NPs.[33] At the same time, the interaction between GO and TiO_2 requires further investigation to understand how doping affects electron transport properties in perovskite solar cells.[34] Thus, despite these advances, gaps remain: the effects of GO doping on electron transport, as well as consistent control over particle size, crystallinity, and morphology in green synthesis, are still not fully understood. Research combining both Malabar spinach extract and GO doping is notably lacking.

This study seeks to address these gaps by exploring the green synthesis of TiO_2 nanoparticles using Malabar spinach leaf extract, coupled with GO doping. It aims to evaluate how this combined approach influences the characteristics and performance of TiO_2 nanoparticles as an electron transport layer in PSCs. To the best of the authors' knowledge, this is the first investigation to examine these specific variables in tandem.

Materials and methods

Malabar spinach leaf extract preparation

The Malabar spinach (MS) leaf extract was prepared according to the literature with slight modifications.[35] The Malabar spinach leaves obtained from the local market were washed and dried under ambient conditions. Twenty grams of Malabar spinach leaves were placed in a beaker and crushed before being added with two solvent variations: distilled water (DW) only or a combination of 1:1 distilled water and ethanol (DWE) to form a 100 mL mixture. The mixture was agitated for 2 hours using a magnetic stirrer, then filtered to obtain Malabar spinach leaf extract. The extract was stored in a dark bottle for further use or characterization.

Green synthesis procedure

The environmentally friendly synthesis of titanium dioxide using MS leaf extract as a medium was conducted via the sol-gel method with slight modifications.[36] The procedure is explained as follows. Eight beaker glasses were prepared, and 10 mL of titanium tetra isopropoxide (TTIP, $Ti\{OCH(CH_3)_2\}_4$, Sigma Aldrich) was poured into each beaker glass.

Table 1. Solvent variations, doping, and sample codes for the green synthesis. Commercial TiO_2 P25 was used as a comparison.

Solvent	Blank	MS	GO	MS/GO
Distilled Water (DW)	1A	1B	1C	1D
Distilled Water + Ethanol (1:1) (DWE)	2A	2B	2C	2D

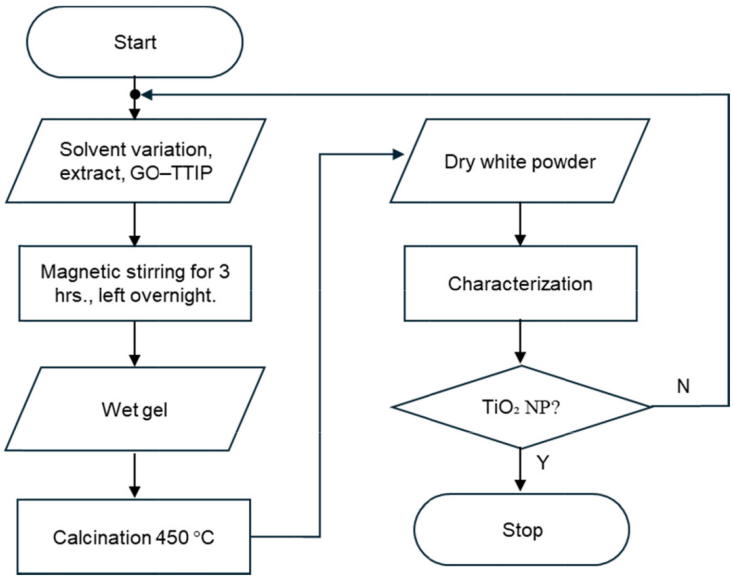

Fig. 1. Flowchart for the green synthesis of TiO_2 NPs preparation steps.

Different solvent variation was added dropwise to each beaker: distilled water only (DW), mixture of 1:1 distilled water and ethanol (DWE), Malabar spinach leaf extracted using distilled water only (DW/MS), Malabar spinach leaf extracted using distilled water + ethanol (DWE/MS), distilled water only with the addition of GO (DW/GO), mixture of 1:1 distilled water and ethanol with the addition of GO (DWE/GO), Malabar spinach leaf extracted using distilled water with the addition of GO (DW/MS/GO), and Malabar spinach leaf extracted using distilled water + ethanol with the addition of GO (DWE/MS/GO). A commercial TiO_2 P25 was used as a reference. For the sample with GO addition, 0.08 mg/mL GO was dispersed in 125 mL of deionized water and sonicated for 30 minutes. 5 mL of this dispersion was mixed with 5 mL of distilled water or 5 mL of a 1:1 mixture of distilled water and ethanol. See Table 1 for more details on the solvent variation, doping, and sample code. The mixture was agitated using a magnetic stirrer for 3 hours, then left overnight and filtered to obtain a wet gel. The gel was dried at 100 ˚C for 1 hour before being calcined at 450 ˚C for 2 hours. The dry white powders of TiO_2 NPs obtained through green synthesis with various solvent variations and/or dopants are ready for further treatment and characterization. The flowchart for the green synthesis steps is provided in Fig. 1.

Application in perovskite solar cell

Photocurrent characteristics of the TiO_2 NPs were revealed by measuring the relationship between the voltage, current, and power output under different conditions in a perovskite solar cell (PSC) device. The PSC device was fabricated according to the literature, as explained in the following.[37,38] The TiO_2 NPs were first deposited as electron transport layers on an indium tin oxide (ITO) glass substrate using the doctor-blade method. Further, the perovskite compound was coated on top of the TiO_2 NPs layer. The process began with the preparation of perovskite materials, which consisted of methylammonium iodide (CH_3NH_3I, MAI), PbI_2, and $ZnCl_2$ in a molar ratio of 1:3:1. The perovskite materials were then dissolved in dimethyl sulfoxide (DMSO). The MAI-PbI_2-$ZnCl_2$-DMSO solution was then deposited on the TiO_2 NPs layer from the previous stage using the doctor-blade method. After the deposition, 100 μL of chlorobenzene was dropped and left for 20 seconds before heating to 100 ˚C for 5 minutes. In the next step, the hole transport layer was prepared. The procedure involved dissolving 72.3 mg of Spiro-OMeTAD in 1 mL of chlorobenzene. The solution was deposited on top of the perovskite layer using the same doctor-blade method, then air-dried. At the final step, the gold layer was deposited using a gold coater for 2 minutes,

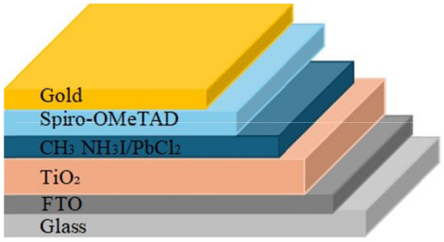

Fig. 2. Schematic diagram of the PSC device stacking layers.

and then the sample was left for 2 hours before characterization of the photocurrent. The schematic of the PSC device, showing the stacking layers, is illustrated in Fig. 2.

Characterization

All characterizations were performed under ambient conditions. The functional groups of Malabar spinach leaf extract were examined using Fourier transform infrared spectroscopy (FTIR, PerkinElmer ATR Spectrum One). The infrared characteristics of TiO_2 NPs were also analyzed using FTIR to assess the effect of the medium on the green synthesis process. Furthermore, the optical characteristics were evaluated using ultraviolet-visible diffuse reflectance spectroscopy (UV-Vis DRS, Shimadzu UV2450), crystallographic information was revealed using X-ray diffraction (XRD, AERIS Malvern PANalytical), and the surface morphology and the elemental composition were analyzed using field emission scanning electron microscopy equipped with energy dispersive X-ray spectroscopy (FESEM/EDS, FEI Inspect F50). The performance of the PSC device was then characterized using a source meter coupled with a solar simulator (Keithley 2450/ABET Sunlite™) at 100 mW/cm^2.

Results and discussion

Infrared characteristics

The infrared spectra of Malabar spinach leaf extracts with different solvent variations are given in Fig. 3(a), whereas the infrared spectra of TiO_2 NPs are presented in Fig. 3(b). The infrared spectra of Malabar spinach extract show several absorption bands. As shown in Fig. 3(a), all spectra show the presence of hydrogen-bonded OH stretching from 3600 to 3000 cm^{-1} and C–H stretching from 2973 to 2878.[39] The weak absorption at 2140–2100 cm^{-1} corresponds to C≡C from alkyne. The region at 1710 cm^{-1} indicates the presence of C=O from conjugated aldehyde, and 1630 cm^{-1} suggests the presence of C=C stretching vibration from alkene. The regions at 1423–1274 cm^{-1} belong to an aromatic compound. The area at 1100 corresponds to C–O from alcohol, whereas the stretching vibration of the C–O–C esters is found at 1046 cm^{-1}. The sharp absorption at around 985–995 cm^{-1} suggests the presence of C=C bending from an alkene. It is expected that the presence of these functional groups in the form of carboxyl and or hydroxyl groups in the extracts will interact and bind to the TiO_2 surface, affecting growth during the reaction process.[40]

As indicated in Fig. 3(b), commercial TiO_2 P25 shows several weak absorption bands at around 3600–3000 and 650 cm^{-1} as indications of stretching vibrations from hydrogen-bonded water and hydroxyl groups and the bridging stretching mode of Ti-O-Ti, respectively.[41] The presence of OH groups is expected from the interaction of TiO_2 NPs with environmental moisture.[42] The spectra of TiO_2 NPs obtained from the green synthesis with different solvents and GO doping, the characteristics follow that of commercial TiO_2 with the addition of a weak

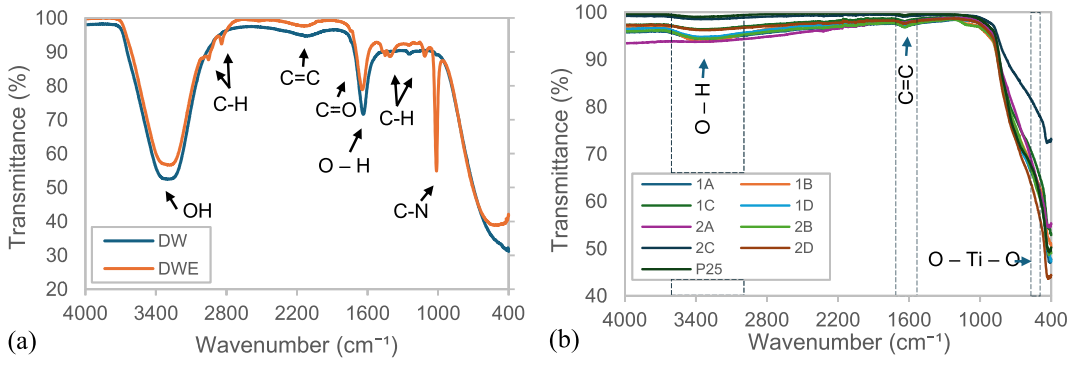

Fig. 3. Infrared spectra of (a) Malabar spinach leaf extract using different solvents and (b) TiO_2 NPs synthesized using solvent variations: distilled water (1A), distilled water/Malabar spinach leaf extract (1B), distilled water + ethanol (2A), distilled water + ethanol/Malabar spinach leaf extract (2B), distilled water/graphene oxide (1C), distilled water/Malabar spinach leaf extract/graphene oxide (1D), distilled water + ethanol/graphene oxide (2C), and distilled water + ethanol/Malabar spinach leaf extract/graphene oxide (2D).

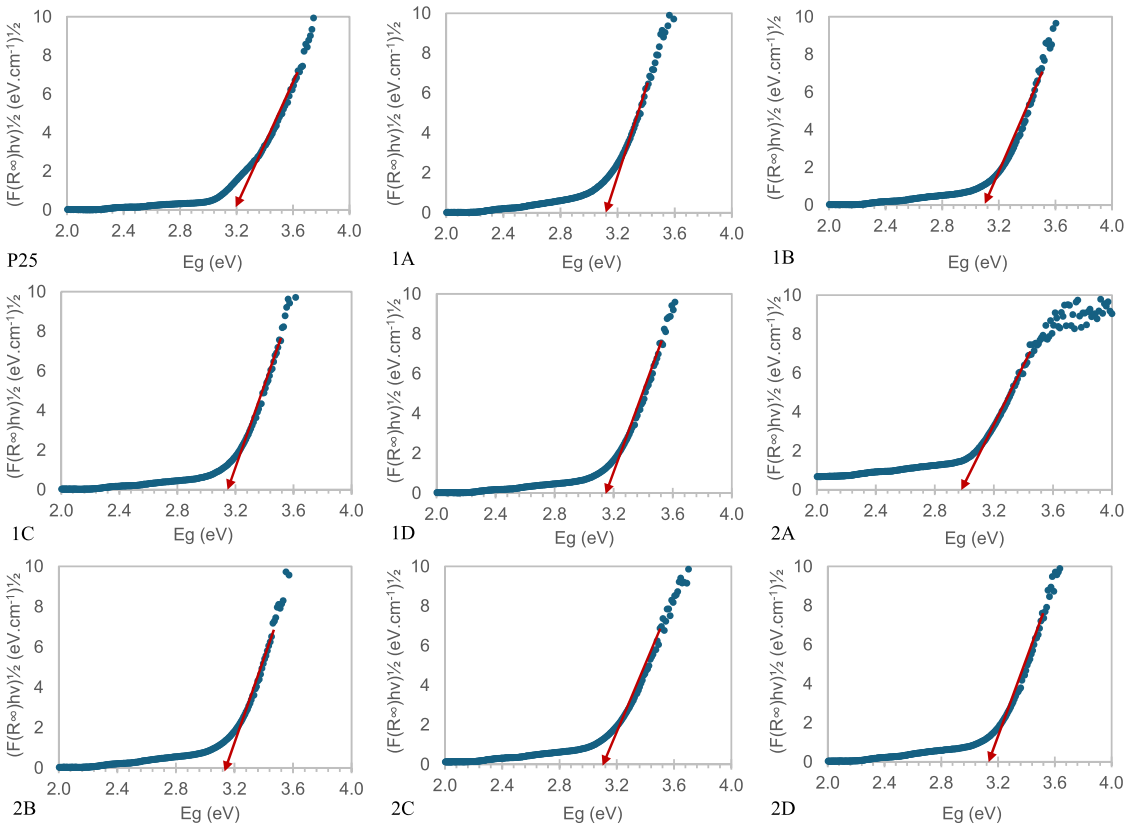

Fig. 4. Tauc plots for bandgap energy determination of commercial TiO_2 (P25) and those synthesized using solvent variations: distilled water (1A), distilled water/Malabar spinach leaf extract (1B), distilled water + ethanol (2A), distilled water + ethanol/Malabar spinach leaf extract (2B), distilled water/graphene oxide (1C), distilled water/Malabar spinach leaf extract/graphene oxide (1D), distilled water + ethanol/graphene oxide (2C), and distilled water + ethanol/Malabar spinach leaf extract/graphene oxide (2D).

absorption band at around 1630 cm^{-1} from stretching vibrations of the C=C group. It has been confirmed that the green-synthesized product is TiO_2 nanoparticles with a slight amount of environmental moisture.

Optical characteristics

The specimens were characterized using UV-Vis DRS, and the obtained spectra, as shown in Fig. S1 in the supplementary information, were further analyzed to reveal the optical characteristics of TiO_2 NPs. Optical characteristics, such as absorption, complex refractive index, and electron transition, depend on the material's bandgap energy.[43] The bandgap energies were calculated using the Kubelka–Munk relation given in Eq. (1),[44]

$$\left(F\left(R_\infty\right).h\nu\right)^{\frac{1}{\gamma}} = B\left(h\nu - E_g\right) \quad (1)$$

In this Kubelka–Munk expression, the γ factor will depend on the electron transition mode. For a direct transition, the γ value is $1/2$, whereas for an indirect transition, the γ value is 2. Further, the factor F(R∞) is expressed as in Eq. (2),

$$F\left(R_\infty\right) = \left(1 - R_\infty\right)^2 / \left(2R_\infty\right) \quad (2)$$

where R∞ is the reflectance from the UV-DRS examination. The bandgap energy was further determined by fitting the data into a Tauc plot $(F(R\infty).hc/\lambda)^{1/2}$ vs hc/λ assuming an indirect allowed transition bandgap energy.[45] The results are illustrated in Fig. 4. The bandgap energy for each NP was then obtained by extrapolating the linear portion of the Tauc plot to the intersection point on the *x*-axis.

The bandgap energy for commercial TiO_2 (P25) is 3.2000 eV, consistent with our previous results.[26] For TiO_2 NPs synthesized using distilled water only (1A), the bandgap energy is 3.1800 eV. In contrast, the bandgap energy of those synthesized using Malabar spinach leaf extract (1B), GO-doped (1C), and a combination of GO-doped and green-synthesized using Malabar spinach leaf extract (1D) remains at 3.1600 eV. It can be observed that the bandgap energy decreases slightly with the use of a green medium and/or GO doping. Notably, TiO_2 NPs synthesized with distilled water + ethanol (2A) exhibit

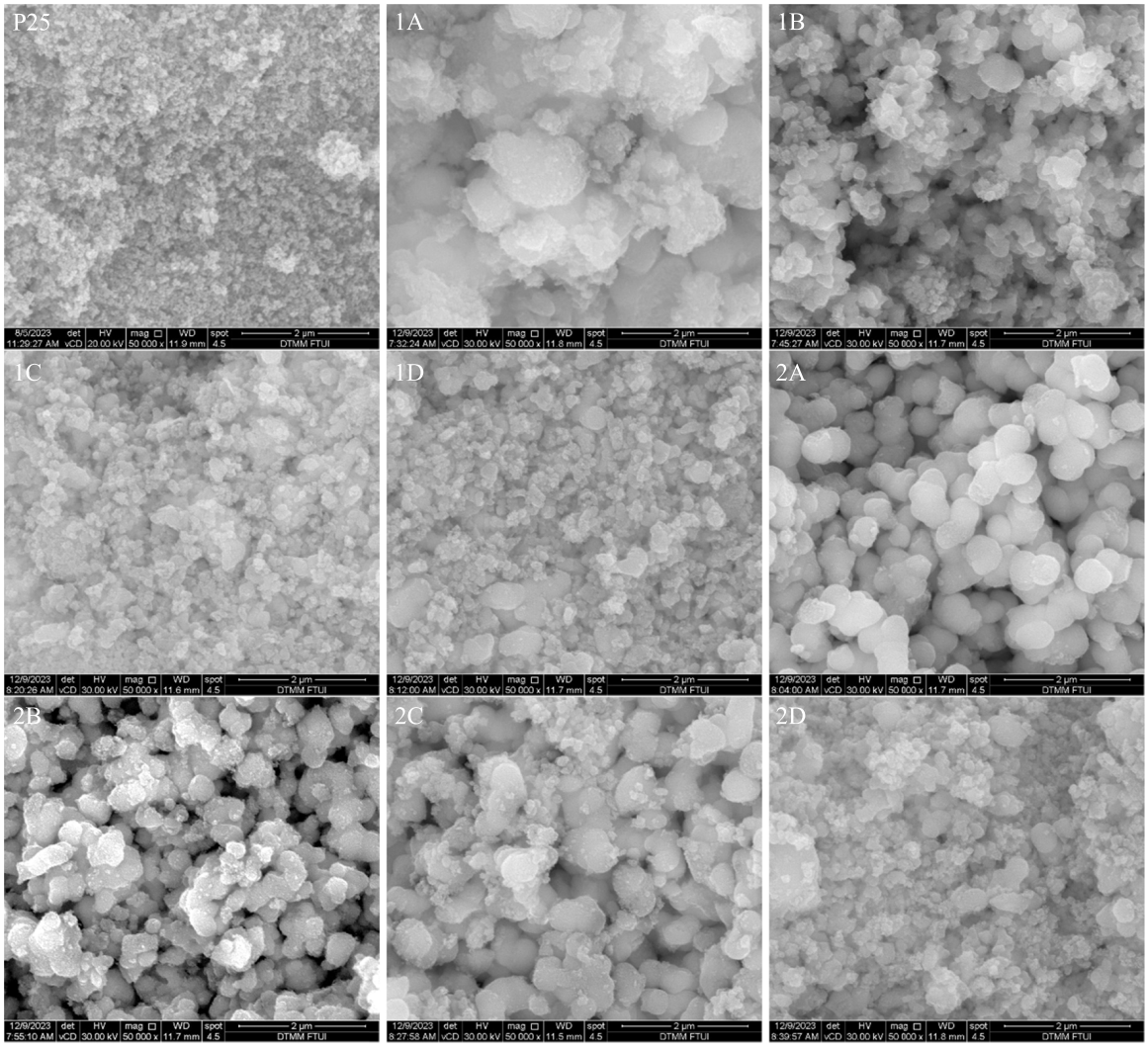

Fig. 5. Electron images of commercial TiO_2 (P25) and those synthesized using solvent variations: distilled water (1A), distilled water/Malabar spinach leaf extract (1B), distilled water + ethanol (2A), distilled water + ethanol/Malabar spinach leaf extract (2B), distilled water/graphene oxide (1C), distilled water/Malabar spinach leaf extract/graphene oxide (1D), distilled water + ethanol/graphene oxide (2C), and distilled water + ethanol/Malabar spinach leaf extract/graphene oxide (2D).

a significant decrease in bandgap energy (3.0400 eV) compared to other samples: 2B is 3.1600 eV, 2C is 3.1200 eV, and 2D is 3.1700 eV. Based on these values, it is confirmed that the lowest bandgap energy was obtained from the solvent combination of distilled water and ethanol, which is consistent with the previous result. [46]

Surface morphology and elemental composition

Surface morphology of TiO_2 NPs was elucidated using field emission SEM, and the results are provided in Fig. 5. In contrast, the results from the elemental composition characterized using EDX are given in Table 2. To better understand the characteristics of the synthesized TiO_2 nanoparticles, the particle size and porosity of each sample were analyzed using ImageJ.

As shown in Fig. 5, the morphology of the sample synthesized with distilled water only (1A) shows a rugged appearance, tending to agglomerate, with an average particle size of 280 nm. In contrast, those synthesized using distilled water and Malabar spinach extract (1B) exhibit a finer, sand-like texture with reduced agglomeration, characterized by an average particle size of 123 nm. The particle size of GO-doped TiO_2, synthesized using only distilled water, shows notable differences, with smaller, more homogeneous particles of 75 nm and 72 nm for 1C and 1D, respectively. The samples synthesized using a mixture of distilled water and ethanol (2A) produced more uniformly distributed nanostructures,

Table 2. Elemental composition of commercial TiO_2 (P25) and those synthesized using solvent variations: distilled water (1A), distilled water/Malabar spinach leaf extract (1B), distilled water + ethanol (2A), distilled water + ethanol/Malabar spinach leaf extract (2B), distilled water/graphene oxide (1C), distilled water/Malabar spinach leaf extract/graphene oxide (1D), distilled water + ethanol/graphene oxide (2C), and distilled water + ethanol/Malabar spinach leaf extract/graphene oxide (2D).

	Wt.%								
Element	P25	1A	1B	1C	1D	2A	2B	2C	2D
C	-	-	-	1.6000	1.2900	-	-	1.4900	1.4200
O	29.6100	38.1100	34.8800	32.0800	31.9200	36.0500	33.8300	32.1300	38.6800
Ti	70.3900	61.8900	65.1200	66.3300	66.7800	63.9500	66.1700	66.3800	59.8900

albeit with larger particle sizes (262 nm), compared to those synthesized using Malabar spinach leaf extract alone (2B), which produced 128 nm particles. The samples synthesized using a mixture of distilled water and ethanol with GO addition (2C), with an average particle size of 139 nm, appear to be more diverse compared to those synthesized using Malabar spinach leaf extract with GO addition (2D), with an average particle size of 150 nm. For comparison, the commercial TiO_2 (P25) exhibits sphere-like particles that tend to form agglomerates but with a homogeneous average particle size of 26 nm, consistent with our previous finding.[26]

Meanwhile, the porosity measured using ImageJ also shows the same trend: the larger the particle size, the greater the porosity. The porosity of the sample synthesized using distilled water only (1A) is 21%. In contrast, those synthesized using distilled water and Malabar spinach extract (1B), which display a finer, sand-like texture and less agglomeration, have a porosity of 19%. The GO-doped TiO_2, synthesized using only distilled water, has a porosity of 13% and 10% for samples 1C and 1D, respectively. The samples synthesized using a mixture of distilled water and ethanol (2A) have a porosity of 16%, whereas those synthesized using Malabar spinach leaf extract only (2B) have a porosity of 21%. The samples synthesized using a mixture of distilled water and ethanol with GO addition (2C) have a porosity of 27%, compared to those synthesized using Malabar spinach leaf extract with GO addition (2D), with a porosity of 17%. The commercial TiO_2 (P25) exhibits the lowest porosity of all, at 7%, consistent with its small particle size.

A study by Dey and Srivasta found a strong connection between morphology and structure in SEM images, linking them and revealing the material's properties.[47] They demonstrated that the rutile phase, characterized by a tetragonal structure, is associated with a uniform spherical morphology (120–160 nm), as observed in SEM and TEM images. Another study by Estrada-Flores et al. demonstrated a relationship among morphology, porosity, and the photocatalytic activity of TiO_2 prepared by the sol-gel method.[48] They demonstrated that the spherical morphology and porosity of mesoporous nanoparticles, related to the anatase phase, enhanced the absorption of light in the visible region. It is worth noting that morphology can impact porosity and connectivity, thereby influencing the material's structural stability, which, in turn, affects its performance in a specific application.

For the elemental composition, as shown in Table 2, the composition of titanium ranges from 59.89–70.39 wt.%, whereas oxygen ranges from 29.61–38.68 wt.%, which confirms the successful process of the green synthesis of TiO_2 NPs using Malabar spinach leaf extract as a medium and capping agent, and the use of GO as a dopant.[49] The presence of carbon elements in samples 1C-D and 2C-D can be understood since they contain GO as a dopant.

Crystallographic properties

The crystallographic properties of TiO_2 NPs were examined using the powder X-ray diffraction technique. The results are provided in Fig. 6. The diffractogram of commercial TiO_2 (P25) shows the prominent peaks centering at 2θ positions 25.30°, 38.40°, 48.10°, 55.00°, 62.60°, 68.70°, 74.00° indicating the presence of (101), (004), (200), (211), (204), (116) and (215) planes, respectively, of tetragonal anatase phase with space group $I4_1/amd$ (ICSD 98-015-4604).[19,20] Other less prominent peaks are detected at 27.32°, 35.84°, 41.12°, and 41.12°, indicating the presence of (110), (101), (111), and (120) planes, respectively, of the tetragonal rutile phase with space group $P4_2/mnm$ (ICSD 98-003-3839). All diffractograms from the synthesis also reveal prominent peaks indicating a pure anatase phase (ICSD 98-009-2363), except for TiO_2 NPs synthesized using distilled water only (1A), where the second phase of brookite is detected at 2θ 31.60° (ICSD 98-015-4605).[50] The second phase, with a rutile structure, is also detected from the green synthesis using only a mixture of distilled water and ethanol (2A). These findings agree with those of others and confirm our previous work.[26,51] Further analysis was conducted using Rietveld refinement to determine the crystallographic

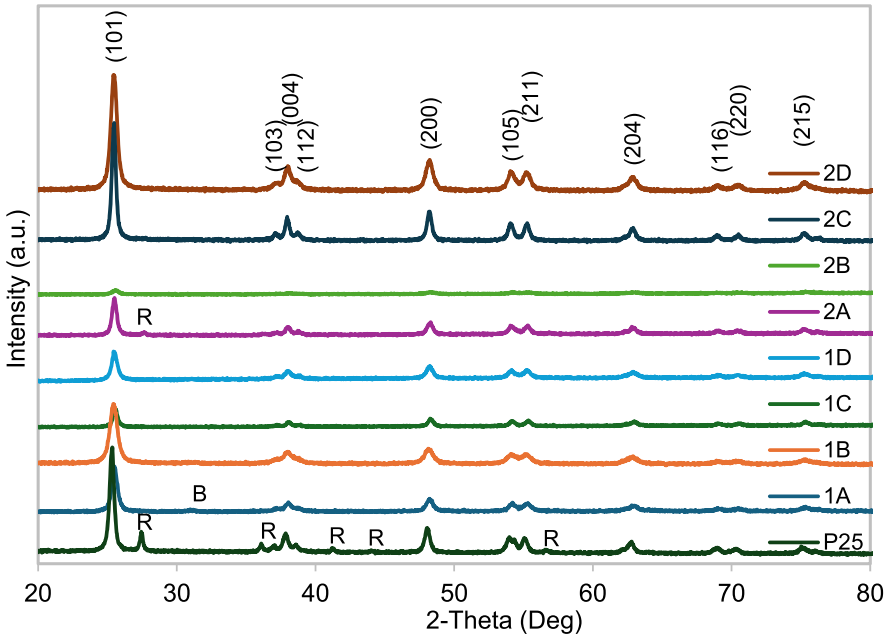

Fig. 6. X-ray diffractograms of commercial TiO_2 (P25) and those synthesized using solvent variations: distilled water (1A), distilled water/Malabar spinach leaf extract (1B), distilled water + ethanol (2A), distilled water + ethanol/Malabar spinach leaf extract (2B), distilled water/graphene oxide (1C), distilled water/Malabar spinach leaf extract/graphene oxide (1D), distilled water + ethanol/graphene oxide (2C), and distilled water + ethanol/Malabar spinach leaf extract/graphene oxide (2D).

Table 3. Lattice parameters of commercial TiO_2 (P25) and those synthesized using solvent variations: distilled water (1A), distilled water/Malabar spinach leaf extract (1B), distilled water + ethanol (2A), distilled water + ethanol/Malabar spinach leaf extract (2B), distilled water/graphene oxide (1C), distilled water/Malabar spinach leaf extract/graphene oxide (1D), distilled water + ethanol/graphene oxide (2C), and distilled water + ethanol/Malabar spinach leaf extract/graphene oxide (2D).

Sample	Lattice parameter			Goodness of fit (χ^2)	Crystallite size (nm)
	a (Å)	c (Å)	V $(Å)^3$		
P25	3.7864(2)	9.5072(6)	136.3031	1.8500	18.0000
1A	3.7888(6)	9.5060(1)	136.4541	1.7400	15.2700
1B	3.7881(5)	9.5010(1)	136.3398	1.4100	9.4600
1C	3.7863(5)	9.5110(1)	136.3561	1.5600	35.0900
1D	3.7895(7)	9.5110(2)	136.5844	2.0300	16.1800
2A	3.7882(5)	9.5120(1)	136.4364	1.9900	24.8600
2B	3.7900(1)	9.5050(4)	136.5388	1.0800	22.5000
2C	3.7858(3)	9.5121(7)	136.3279	1.9900	21.8500
2D	3.7871(3)	9.5068(7)	136.3514	1.1800	13.9900

properties, including lattice parameters and crystallite size. The Rietveld refinement summary is given in Table 3. As shown in Table 3, the average crystalline size ranges from the smallest size of 9.46 nm observed in the sample synthesized using Malabar spinach leaf extract to the largest crystallite size of 35.09 nm obtained from the one synthesized using a combination of Malabar spinach leaf extract + GO with the solvent of distilled water only.

Photocurrent characteristics

Photocurrent activities are revealed by analyzing the relation between current and voltage (I-V) as shown in Fig. 7(a), current density and voltage (J-V) as shown in Fig. 7(b), and power density and voltage (P-V) as shown in Fig. 7(c). The power conversion efficiency (PCE) of the PSC device was calculated by examining the J-V curve. The summary of the performance characteristics is presented in Table 4. The PSC device fabricated from the commercial TiO_2 P25 has a PCE of 0.026%. For the device fabricated from TiO_2 NPs obtained via regular synthesis without a green medium, the PCE is 0.062% (1A) and 0.008% (2A). For the PSC device fabricated using TiO_2 NPs obtained via green synthesis with Malabar spinach leaf extract only, the PCE is 0.006% (1B) and 0.036% (2B). For the PSC device fabricated with TiO_2 NPs

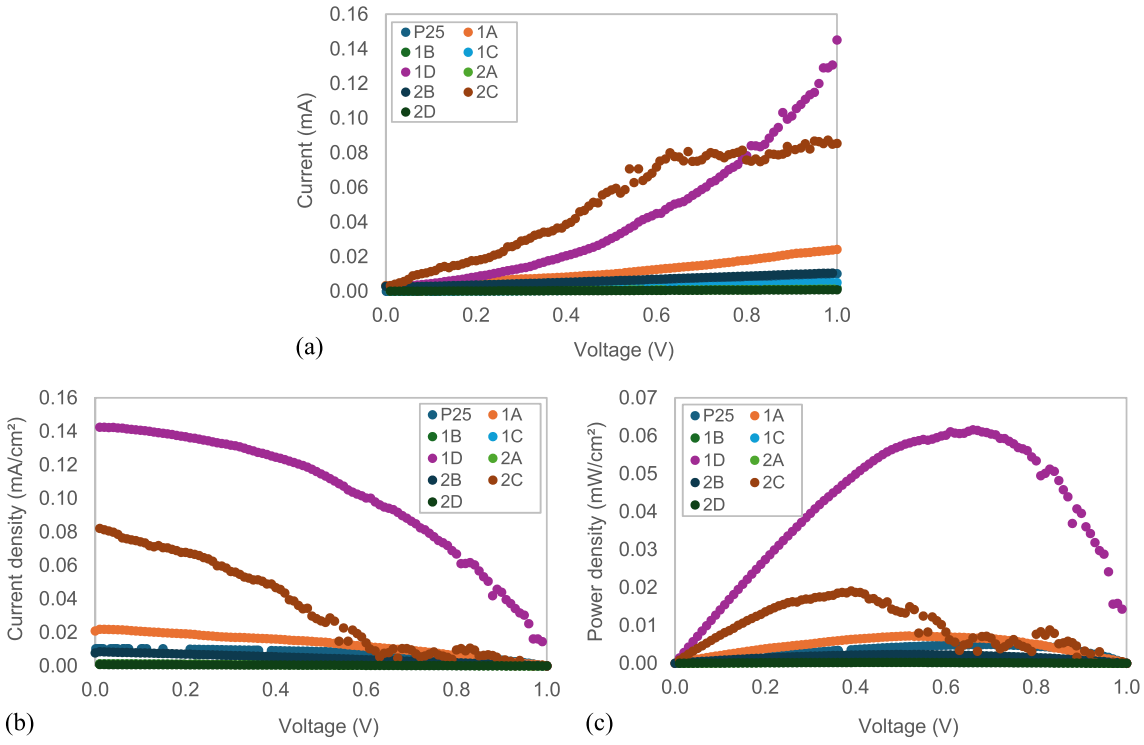

Fig. 7. Characteristics (a) I-V, (b) J-V, and (c) P-V curves of the PSC devices fabricated from commercial TiO_2 (P25) and those synthesized using solvent variations: distilled water (1A), distilled water/Malabar spinach leaf extract (1B), distilled water + ethanol (2A), distilled water + ethanol/Malabar spinach leaf extract (2B), distilled water/graphene oxide (1C), distilled water/Malabar spinach leaf extract/graphene oxide (1D), distilled water + ethanol/graphene oxide (2C), and distilled water + ethanol/Malabar spinach leaf extract/graphene oxide (2D).

and no green medium, but with GO addition only, the PCE is 0.009% (1C) and 0.198% (2C). For the PSC device fabricated using TiO_2 NPs from the combination of green synthesis using Malabar Spinach leaf extract and GO addition, the PCE is 0.247% (1D) and 0.002% (2D). The PCE value decreases with the combination of Malabar spinach leaf extract prepared with both distilled water and ethanol, and GO addition. This combination may increase resistance in the electron transport layer; however, the exact mechanism has yet to be confirmed. Nevertheless, the best performance was achieved in this work with the PSC device fabricated using green-synthesized TiO_2 NPs, prepared from Malabar spinach leaf extracts and water, with the addition of GO.

Although the PCE obtained in this work is still relatively low, the current results using natural plant extracts are promising, particularly for developing eco-friendly green synthesis combined with graphene oxide addition. To compare with the PCE values obtained in this work, Table 5 presents the methods used to synthesize TiO_2 NPs and their corresponding

Table 4. Power conversion efficiency of the PSC device fabricated from commercial TiO_2 (P25) and those synthesized using solvent variations: distilled water (1A), distilled water/Malabar spinach leaf extract (1B), distilled water + ethanol (2A), distilled water + ethanol/Malabar spinach leaf extract (2B), distilled water/graphene oxide (1C), distilled water/Malabar spinach leaf extract/graphene oxide (1D), distilled water + ethanol/graphene oxide (2C), and distilled water + ethanol/Malabar spinach leaf extract/graphene oxide (2D).

Sample	V_{oc} (V)	J_{sc} (mA/cm^2)	V_{max} (V)	I_{max} (mA)	PCE (%)
P25	0.9900	0.0100	0.7300	0.0035	0.0259
1A	0.9500	0.0024	0.5500	0.0113	0.0620
1B	0.9000	0.0020	0.4900	0.0012	0.0059
1C	0.9000	0.0050	0.5900	0.0016	0.0094
1D	0.9000	0.1290	0.5800	0.0425	0.2467
2A	0.9000	0.0012	0.8228	0.0009	0.0077
2B	0.8000	0.0107	0.5500	0.0065	0.0355
2C	0.9000	0.0854	0.4300	0.0459	0.1976
2D	0.9800	0.0009	0.4700	0.0004	0.0018

Table 5. A comparative table of the method used in synthesizing TiO_2 NPs and their efficiency for solar cell applications: dye-sensitized solar cell (DSSC) and perovskite solar cell (PSC).

Method	Precursor	Variation	Application	PCE (%)
Green synthesis using *Saccharum officinarum*[52]	Titanium butoxide	Water	DSSC	0.6800
		Water + sugarcane juice	DSSC	1.2900
		Sugarcane juice	DSSC	3.6500
Green synthesis using *Calotropis gigantea*[53]	$TiCl_4$	Leaf in water	DSSC	0.0182
		Flowers in water	DSSC	0.0019
		Seeds in water	DSSC	0.0039
Green synthesis using *Citrus limon*[30]	Titanium butoxide	0.9% juice extract	DSSC	3.8700
		0.45% juice extract	DSSC	4.5500
		0.27% juice extract	DSSC	2.7300
Green synthesis using *Bixa orellana*[54]	Titanium butoxide	Seeds in ethanol	DSSC	2.9700
Green synthesis using *Terminalia catappa*[19]	TTIP	Fruits in ethanol	DSSC	1.3800
		Fruits in ethanol + GO	DSSC	1.4600
Laser Pyrolisis[55]	TTIP	TiO_2	PSC	11.4000
		TiO_2 + Graphene	PSC	12.3000
Low temperature plasma[56]	Titanium Diisopropoxide	Plasma treated 16 s	PSC	4.8900
		Plasma treated 32 s	PSC	9.0000
		Plasma treated 64 s	PSC	11.7600
Conventional sol-gel[57]	$TiCl_4$	TiO_2	PSC	17.8600
		TiO_2 + 1% Nb	PSC	18.4100
		TiO_2 + 3% Nb	PSC	18.9700
		TiO_2 + 5% Nb	PSC	18.2200

PCE values for various solar cell applications. Since there is no available literature on the green synthesis of TiO_2 NPs with perovskite solar cells, the application in dye-sensitized solar cells (DSSCs) is presented instead.

Conclusion

This study demonstrated that green-synthesized TiO_2 nanoparticles, particularly those prepared using Malabar spinach leaf extract and graphene oxide (GO), predominantly exhibited the anatase phase with varying crystallite sizes and morphologies. The samples synthesized using distilled water and ethanol generally showed reduced crystallite sizes, while SEM analysis revealed differing levels of agglomeration, with minimal morphological disruption from the plant extract. UV-Vis spectrometry indicated that green synthesis and GO doping subtly lowered the bandgap energy to approximately 3.1600 eV, with a more pronounced decrease observed in TiO_2 synthesized using a mixture of distilled water and ethanol (3.0400 eV). This lower bandgap could enhance light absorption, though it did not consistently translate into better device performance. Photovoltaic testing revealed significant variation in PCE, with the highest efficiency (0.2467%) achieved by TiO_2 synthesized using distilled water, Malabar spinach extract, and GO, highlighting a synergistic effect between green reductants and GO doping. In contrast, the lowest efficiency (0.0018%) was observed in the ethanol-based green synthesis with GO, indicating that solvent interactions significantly influence charge transport properties. Overall, green synthesis—especially when combined with GO—presents a viable strategy for producing efficient, sustainable TiO_2-based materials for perovskite solar cells. These findings offer insight and may pave the way for more novel, environmentally friendly methods in synthesizing nanomaterials for a sustainable future. Green synthesis methods utilize naturally reducing and capping agents, thereby eliminating the need for toxic chemicals and making the process safer for both the environment and human health. At the same time, since TiO_2 NPs are widely used as an electron transport layer in perovskite solar cell applications, the green synthesis would make these applications more sustainable and cost-effective. However, further research is required to control nanoparticle morphology and optimize synthesis conditions, particularly considering the compositional variability of plant-derived reducing agents.

Acknowledgement

The authors acknowledge funding from Fakultas Teknik Universitas Indonesia through the Hibah Seed Funding Lektor Kepala, with the grant number specified in the funding details.

Authors' declaration

- Conflicts of Interest: None.
- We hereby confirm that all the Figures and Tables in the manuscript are ours. Furthermore, any Figures and images that are not ours have been included with the necessary permission for republication, which is attached to the manuscript.
- No animal studies are present in the manuscript.
- No human studies are present in the manuscript.
- Ethical Approval: The project was approved by the local ethical committee at Universitas Indonesia, Indonesia.

Authors' contributions statement

N. S. : conceptualization, funding acquisition, methodology, formal analysis, validation, writing – original draft, review, and editing. I. P. W. : investigation and data curation. F. A. : investigation and data curation. A. R.: investigation, data curation, and visualization. A. H. Y.: writing – review and editing. D. D.: writing – review and editing.

Data availability

Data will be made available upon request.

Funding statement

Fakultas Teknik Universitas Indonesia, Grant No. NKB-3427/UN2.F4.D/PPM.00.00/2024.

Supplementary materials

Supplementary materials is available at https://doi.org/10.21123/2411-7986.-7.

References

1. Min J, Yan G, Abed AM, Elattar S, Khadimallah MA, Jan A, *et al.* The effect of carbon dioxide emissions on the building energy efficiency. Fuel. 2022 Oct 15 [cited 2025 Feb 24];326. https:/doi.org/10.1016/j.fuel.2022.124842.
2. Kober T, Schiffer HW, Densing M, Panos E. Global energy perspectives to 2060 – WEC's World Energy Scenarios 2019. Energy Strat Revs. 2020 Sep 01 [cited 2025 Feb 24];31. https://doi.org/10.1016/j.esr.2020.100523.
3. Filonchyk M, Peterson MP, Zhang L, Hurynovich V, He Y. Greenhouse gases emissions and global climate change: Examining the influence of CO_2, CH_4, and N_2O. Sci Total Env. 2024 July 20 [cited 2025 Feb 24];935. https://doi.org/10.1016/j.scitotenv.2024.173359.
4. Guo YY, Lightfoot P. Structural diversity of lead halide chain compounds, $APbX_3$, templated by isomeric molecular cations. Dalton Trans. 2020 Aug 27 [cited 2025 Feb 24];49(36): 12767–12775. https://doi.org/10.1039/D0DT02782K.
5. Yang Y, Hoang MT, Bhardwaj A, Wilhelm M, Mathur S, Wang H. Perovskite solar cells based self-charging power packs: Fundamentals, applications and challenges. Nano Energy. 2022 Apr 01 [cited 2025 Feb 24];94. https://doi.org/10.1016/j.nanoen.2021.106910.
6. Lohmann KB, Motti SG, Oliver RDJ, Ramadan AJ, Sansom HC, Yuan Q, *et al.* Solvent-Free Method for Defect Reduction and Improved Performance of p-i-n Vapor-Deposited Perovskite Solar Cells. ACS Energy Lett. 2022 June 10 [cited 2025 Feb 24];7(6):1903–1911. https://doi.org/10.1021/acsenergylett.2c00865.
7. Zheng D, Yang X, Čuček L, Wang J, Ma T, Yin C. Revolutionizing dye-sensitized solar cells with nanomaterials for enhanced photoelectric performance. J Clean Prod. 2024 July 20 [cited 2025 June 26];464. https://doi.org/10.1016/j.jclepro.2024.142717.
8. Hendi AA, Alanazi MM, Alharbi W, Ali T, Awad MA, Ortashi KM, *et al.* Dye-sensitized solar cells constructed using titanium oxide nanoparticles and green dyes as photosensitizers. J King Saud Univ Sci. 2023 April 01 [cited 2025 June 26];35(3). https://doi.org/10.1016/j.jksus.2023.102555.
9. Aboulouard A, Gultekin B, Can M, Erol M, Jouaiti A, Elhadadi B, *et al.* Dye sensitized solar cells based on titanium dioxide nanoparticles synthesized by flame spray pyrolysis and hydrothermal sol-gel methods: A comparative study on photovoltaic performances. J Mater Res Technol. 2020 Mar 01[cited 2025 June 26];9(2):1569–1577. https://doi.org/10.1016/j.jmrt.2019.11.083.
10. Saraf S, Giraldo M, Paudel HP, Sakthivel TS, Shepard C, Gupta A, *et al.* Photoelectrochemical analysis of band gap modulated TiO_2 for photocatalytic water splitting. Int J Hydrogen Energy. 2017 Apr 13 [cited 2025 June 26];42(15):9938–9944. https://doi.org/10.1016/j.ijhydene.2017.01.232.
11. Sharma R, Khanuja M, Sharma SN, Sinha OP. Reduced band gap & charge recombination rate in Se doped α-Bi_2O_3 leads to enhanced photoelectrochemical and photocatalytic performance: Theoretical & experimental insight. Int J Hydrogen Energy. 2017 Aug 10 [cited 2025 June 26];42(32): 20638–20648. https://doi.org/10.1016/j.ijhydene.2017.07.011.
12. Tahir M, Tasleem S, Tahir B. Recent development in band engineering of binary semiconductor materials for solar driven photocatalytic hydrogen production. Int J Hydrogen Energy. 2020 June 10 [cited 2025 June 26];45(32):15985–16038. https://doi.org/10.1016/j.ijhydene.2020.04.071.
13. Samanta PK. Band gap engineering, quantum confinement, defect mediated broadband visible photoluminescence and associated quantum States of size tuned zinc oxide nanostructures. Optik (Stuttg). 2020 Nov 01 [cited 2025 June 26];221. https://doi.org/10.1016/j.ijleo.2020.165337.
14. Alabdallah NM, Alluqmani SM, Almarri HM, AL-Zahrani AA. Physical, chemical, and biological routes of synthetic titanium dioxide nanoparticles and their crucial role in temperature stress tolerance in plants. Heliyon. 2024 Feb 29 [cited 2025 Feb 24];10(4). https://doi.org/10.1016/j.heliyon.2024.e26537.
15. de Zárate DO, Serna S, Ponce-Alcántara S, Kovylina M, García-Rupérez J. Bottom-up synthesis of mesoporous TiO_2 films for the development of optical sensing layers. Chemosensors. 2021 Dec 01 [cited 2025 Feb 24];9(12). https://doi.org/10.3390/chemosensors9120329.

16. Xu K, Chen J. High-resolution scanning probe lithography technology: a review. Appl Nanosci. 2020 Apr 01 [cited 2025 Feb 24];10(4):1013–1022. https://doi.org/10.1007/s13204-019-01229-5.
17. Duryea D, McKibben N, Manzi J, Brennan T, Subbaraman H, Estrada D, *et al.* Titanium Dioxide Nanomaterial Ink Production Through Laser Ablation Synthesis in Solution for Printed Electronics Applications. Adv Eng Mater. 2024 May 01 [cited 2025 Feb 24];26(10). https://doi.org/10.1002/adem.202400721.
18. Taylor M, Pullar RC, Parkin IP, Piccirillo C. Nanostructured titanium dioxide coatings prepared by Aerosol Assisted Chemical Vapour Deposition (AACVD). J Photochem Photobiol A Chem. 2020 Sep 01 [cited 2025 Feb 24];400. https://doi.org/10.1016/j.jphotochem.2020.112727.
19. Sofyan N, Ridhova A, Yuwono AH, Wu J. Characteristics of Nano Rosette TiO_2 Hydrothermally Grown on A Glass Substrate at Different Reaction Times and Acid Concentrations. Int J Technol. 2018 Dec 07 [cited 2024 Nov 01];9(9):1196–1204. https://doi.org/10.14716/ijtech.v9i6.2345.
20. Sofyan N, Ridhova A, Yuwono AH, Udhiarto A. Preparation of Anatase TiO_2 Nanoparticles Using Low Hydrothermal Temperature for Dye-Sensitized Solar Cell. IOP Conf Ser Mater Sci Eng. 2018 Mar 27 [cited 2024 Nov 01];316. https://doi.org/10.1088/1757-899X/316/1/012055.
21. Pala LPR, Uday V, Gogoi D, Peela NR. Surface and photocatalytic properties of TiO_2 thin films prepared by non-aqueous surfactant assisted sol-gel method. J Environ Chem Eng. 2020 Oct 01 [cited 2025 Feb 24];8(5). https://doi.org/10.1016/j.jece.2020.104267.
22. Ati AA, Abdalsalam AH, Alardhi SM, Dabagh S, Salim A, Ramadhan AA, *et al.* Structural, morphology, magnetic, and electrochemical characterization of pure and magnesium-substituted cobalt ferrite nanoparticles. J Materi Sci: Mater Electron. 2025 Feb 3 [cited 2025 May 1];36(4):252. https://doi.org/10.1007/s10854-025-14331-y.
23. Kumari S, Raturi S, Kulshrestha S, Chauhan K, Dhingra S, András K, *et al.* A comprehensive review on various techniques used for synthesizing nanoparticles. J Mater Res Technol. 2023 Nov 01 [cited 2025 Feb 24];27:1739–1763. https://doi.org/10.1016/j.jmrt.2023.09.291.
24. Eddy DR, Rahmawati D, Permana MD, Takei T, Solihudin, Suryana, *et al.* A review of recent developments in green synthesis of TiO_2 nanoparticles using plant extract: Synthesis, characterization and photocatalytic activity. Inorg Chem Commun. 2024 July 01 [cited 2025 Feb 24];165. https://doi.org/10.1016/j.inoche.2024.112531.
25. Oleiwi HF, Rahma AJ, Salih SI, Beddai AA. Comparative Study of Sol-Gel and Green Synthesis Technique Using Orange Peel Extract to Prepare TiO_2 Nanoparticles. Baghdad Sci J. 2024 Sep 20 [cited 2025 Feb 27];21(5):1702–1711. https://doi.org/10.21123/bsj.2023.8089.
26. Sofyan N, Jamil AM, Ridhova A, Yuwono AH, Dhaneswara D, Fergus JW. Graphene oxide doping in tropical almond (terminalia catappa L.) fruits extract mediated green synthesis of TiO_2 nanoparticles for improved DSSC power conversion efficiency. Heliyon. 2024 Apr 30 [cited 2024 Dec 02];10(8). https://doi.org/10.1016/j.heliyon.2024.e29370.
27. Sofyan N, Rilda Y, Andriayani A, Angellinnov F, M'rad M, Muhammad M, *et al.* Sustainable synthesis of TiO_2 nanoparticles from gambier leaf extract for enhanced DSSC photocurrent response. Results Mater. 2025 Sept 01 [cited 2025 Nov 16];27:100752. https://doi.org/10.1016/j.rinma.2025.100752.
28. Septiningrum F, Yuwono A, Maulana FA, Nurhidayah E, Dhaneswara D, Sofyan N, *et al.* Mangosteen pericarp extract mediated synthesis of Ag/TiO_2 nanocomposite and its application on organic pollutant degradation by adsorption-photocatalytic activity. Curr Res Green Sustain Chem. 2024 Jan 01 [cited 2024 Dec 02];8. https://doi.org/10.1016/j.crgsc.2023.100394.
29. Hussain S, Nazar W, Tajammal A, Nasreen Z, Ahmad T, Asghar A, *et al.* Green Synthesis of TiO_2 Nanoparticle in Morus nigra Leaves; Characterization and Biological Potential. Pol J Environ Stud. 2024 Feb 12 [cited 2024 Dec 02];33(3):2707–2714. https://doi.org/10.15244/pjoes/175060.
30. Singh S, Maurya IC, Tiwari A, Srivastava P, Bahadur L. Green synthesis of TiO_2 nanoparticles using Citrus limon juice extract as a bio-capping agent for enhanced performance of dye-sensitized solar cells. Surf Interfaces. 2022 Feb 01 [cited 2024 Dec 02];28. https://doi.org/10.1016/j.surfin.2021.101652.
31. KoziołŁ, Knap M, Sutor-Świeży K, Górska R, Dziedzic E, Bieniasz M, *et al.* Identification and reactivity of pigments in prominent vegetable leaves of *Basella alba* L. var. "Rubra" (Malabar spinach). Food Chem. 2024 July 01 [cited 2025 Feb 24];445. https://doi.org/10.1016/j.foodchem.2024.138714.
32. Kumar SS, Manoj P, Giridhar P, Shrivastava R, Bharadwaj M. Fruit extracts of *Basella rubra* that are rich in bioactives and betalains exhibit antioxidant activity and cytotoxicity against human cervical carcinoma cells. J Funct Foods. 2015 May 01 [cited 2024 Sep 03];15:509–515. https://doi.org/10.1016/j.jff.2015.03.052.
33. Rommozzi E, Zannotti M, Giovannetti R, D'amato CA, Ferraro S, Minicucci M, *et al.* Reduced graphene oxide/TiO_2 nanocomposite: From synthesis to characterization for efficient visible light photocatalytic applications. Catalysts. 2018 Dec 1 [cited 2025 April 30];8(12). https://doi.org//10.3390/catal8120598.
34. Mahmoud ZH, AL-Salman HNK, Hussein HH, Hsu CY. High-performance TiO_2/perovskite solar cell based GO as hole transport layer. J Mater Sci: Mater Electron. 2024 July 1 [cited 2025 April 30];35(19). https://doi.org/10.1007/s10854-024-12998-3.
35. Ahn EY, Shin SW, Kim K, Park Y. Facile Green Synthesis of Titanium Dioxide Nanoparticles by Upcycling Mangosteen (*Garcinia mangostana*) Pericarp Extract. Nanoscale Res Lett. 2022 Mar 31 [cited 2024 Sep 03];17(1). https://doi.org/10.1186/s11671-022-03678-4.
36. Jassal PS, Kaur D, Prasad R, Singh J. Green synthesis of titanium dioxide nanoparticles: Development and applications. J Agric Food Res. 2022 Aug 23 [cited 2025 Feb 24];10. https://doi.org/10.1016/j.jafr.2022.100361.
37. Dai F, Zhuang Q, Huang G, Deng H, Zhang X. Infrared Spectrum Characteristics and Quantification of OH Groups in Coal. ACS Omega. 2023 May 16 [cited 2025 Feb 24];8(19):17064–17076. https://doi.org/10.1021/acsomega.3c01336.
38. Pydzińska-Białek K, Nowaczyk G, Ziółek M. Complete Perovskite Solar Cells with Gold Electrodes Studied in the Visible and Near-Infrared Ranges. Chem Mater. 2022 July 26 [cited 2025 April 29];34(14):6355–6366. https://doi.org/10.1021/acs.chemmater.2c00845.
39. Noori L, Hoseinpour V, Shariatinia Z. Optimization of TiO_2 paste concentration employed as electron transport layers in fully ambient air processed perovskite solar cells with a low-cost architecture. Ceram Int. 2022 Jan 1 [cited 2025 April 29];48(1):320–336. https://doi.org/10.1016/j.ceramint.2021.09.107.

40. Al-Alwani MAM, Mohamad AB, Kadhum AAH, Ludin NA. Effect of solvents on the extraction of natural pigments and adsorption onto TiO_2 for dye-sensitized solar cell applications. Spectrochim Acta A Mol Biomol Spectrosc. 2015 Feb 13 [cited 2025 Feb 24];138:130–137. https://doi.org/10.1016/j.saa.2014.11.018.
41. Martins NCT, Ângelo J, Girão AV, Trindade T, Andrade L, Mendes A. N-doped carbon quantum dots/TiO_2 composite with improved photocatalytic activity. Appl Catal B. 2016 Sep 15 [cited 2025 Feb 24];193:67–74. https://doi.org/10.1016/j.apcatb.2016.04.016.
42. Zhao Z, Li Z, Zou Z. Understanding the interaction of water with anatase TiO_2 (101) surface from density functional theory calculations. Phys Lett A. 2011 July 25 [cited 2025 Feb 24];375(32):2939–2945. https://doi.org/10.1016/j.physleta.2011.06.022.
43. Miah MH, Khandaker MU, Rahman MB, Nur-E-Alam M, Islam MA. Band gap tuning of perovskite solar cells for enhancing the efficiency and stability: issues and prospects. RSC Adv. 2024 May 16 [cited 2025 Feb 24];14(23):15876–15906. https://doi.org/10.1039/d4ra01640h.
44. Makuła P, Pacia M, Macyk W. How To Correctly Determine the Band Gap Energy of Modified Semiconductor Photocatalysts Based on UV-Vis Spectra. J Phys Chem Lett. 2018 Dec 06 [cited 2025 Feb 24];9(23):6814–6817. https://doi.org/10.1021/acs.jpclett.8b02892
45. Nagaraj G, Raj AD, Irudayaraj AA, Josephine RL. Tuning the optical band Gap of pure TiO_2 via photon induced method. Optik (Stuttg). 2019 Feb 01 [cited 2025 Feb 24];179:889–894. https://doi.org/10.1016/j.ijleo.2018.11.009.
46. Aravind M, Amalanathan M, Mary MSM. Synthesis of TiO_2 nanoparticles by chemical and green synthesis methods and their multifaceted properties. SN Appl Sci. 2021 Apr 01 [cited 2025 Feb 24];3(4). https://doi.org/10.1007/s42452-021-04281-5.
47. Dey B, Srivastava SK. Crystal structure, microstructure, optical, dielectric, and magnetic properties of TiO2 nanoparticles. J Mater Sci: Mater Electron. 2022 Sept 22 [cited 2025 June 24 25];33(30):23506–23514. https://doi.org/10.1007/s10854-022-09111-x.
48. Estrada-Flores S, Martínez-Luévanos A, Perez-Berumen CM, García-Cerda LA, Flores-Guia TE. Relationship between morphology, porosity, and the photocatalytic activity of TiO_2 obtained by sol–gel method assisted with ionic and nonionic surfactants. Bol Soc Esp Cerám Vidrio. 2020 Jan 01 [cited 2025 June 24 25];59(5):209–218. https://doi.org/10.1016/j.bsecv.2019.10.003.
49. Mansoor A, Mehmood M, Ishtiaq M, Jamal A. Synthesis of TiO_2 nanoparticles and demonstration of their antagonistic properties against selected dental caries promoting bacteria. Pak J Med Sci. 2023 Sep [cited 2025 Feb 24];39(5):1249–1254. https://doi.org/10.12669/pjms.39.5.7851.
50. Mishra A, Fischer MKR, Büuerle P. Metal-Free organic dyes for dye-Sensitized solar cells: From structure: Property relationships to design rules. Angewandte Chemie - International Edition. 2009 Mar 23 [cited 2025 Feb 24];48(14):2474–2499. https://doi.org/10.1002/anie.200804709.
51. Iqbal MZ, Ali SR, Khan S. Progress in dye sensitized solar cell by incorporating natural photosensitizers. Sol Energy. 2019 Mar 15 [cited 2025 Feb 24];181:490–509. https://doi.org/10.1016/j.solener.2019.02.023.
52. Singh P, Sharma S, Srivastava P. Natural Saccharum officinarum (sugarcane) juice assisted TiO_2 nanoparticle synthesis for high performance dye-sensitized solar cell. Opt Mater (Amst). 2024 Jan 1 [cited 2025 May 1];147. https://doi.org/10.1016/j.optmat.2023.114685.
53. Pavithra S, Bessy TC, Bindhu MR, Venkatesan R, Parimaladevi R, Alam MM, *et al.* Photocatalytic and photovoltaic applications of green synthesized titanium oxide (TiO_2) nanoparticles by Calotropis gigantea extract. J Alloys Compd. 2023 Oct 15 [cited 2025 May 1];960. https://doi.org/10.1016/j.jallcom.2023.170638.
54. Maurya IC, Singh S, Senapati S, Srivastava P, Bahadur L. Green synthesis of TiO_2 nanoparticles using Bixa orellana seed extract and its application for solar cells. Solar Energy. 2019 July 31 [cited 2025 May 1];194:952–958. https://doi.org/10.1016/j.solener.2019.10.090.
55. Belchi R, Habert A, Foy E, Gheno A, Vedraine S, Antony R, *et al.* One-Step Synthesis of TiO_2/Graphene Nanocomposites by Laser Pyrolysis with Well-Controlled Properties and Application in Perovskite Solar Cells. ACS Omega. 2019 [cited 2025 May 1];4(7):11906–11913. https://doi.org/10.1021/acsomega.9b01352.
56. Homola T, Pospisil J, Shekargoftar M, Svoboda T, Hvojnik M, Gemeiner P, *et al.* Perovskite Solar Cells with Low-Cost TiO_2 Mesoporous Photoanodes Prepared by Rapid Low-Temperature (70 °c) Plasma Processing. ACS Appl Energy Mater. 2020 Dec 20 [cited 2025 May 1];3(12):12009–12018. https://doi.org/10.1021/acsaem.0c02144.
57. Singh R, Ryu I, Yadav H, Park J, Jo JW, Yim S, *et al.* Non-hydrolytic sol-gel route to synthesize TiO_2 nanoparticles under ambient condition for highly efficient and stable perovskite solar cells. Solar Energy. 2019 June 1 [cited 2025 May 1];185:307–314. https://doi.org/10.1016/j.solener.2019.04.066.

التصنيع الأخضر لجسيمات ثاني أكسيد التيتانيوم النانوية باستخدام مستخلص أوراق السبانخ المالاباري المُطعَّم بأكسيد الغرافين لتطبيقات الخلايا الشمسية البيروفسكايتية

نوفريجون صفيان[1،2]، إحسان بندو ويكاكسونو[2]، فيونا أنجيلينوف[2]، أغا ريدهوفا[3]، أحمد هيرمان يونوونو[1،2]، دونانتا دهانيسوارا[1،2]

[1]مركز أبحاث المواد المتقدمة، كلية الهندسة، جامعة إندونيسيا، ديبوك 16424، إندونيسيا.
[2]قسم الهندسة المعدنية وهندسة المواد، كلية الهندسة، جامعة إندونيسيا، ديبوك 16424، إندونيسيا.
[3]مركز أبحاث التعدين، الهيئة الوطنية للبحث والابتكار، تانغيرانغ سيلاتان، بانتن 15314، إندونيسيا.

الملخص

يستقصي هذا البحث مساراً صديقاً للبيئة لتخليق جسيمات ثاني أكسيد التيتانيوم النانوية (TiO_2 NPs) باستخدام مستخلص أوراق السبانخ المالاباري(Basella rubra) ، مع استخدام أكسيد الغرافين (GO) كمادة مطعِّمة، وذلك لتطبيقها كطبقة نقل إلكتروني في الخلايا الشمسية البيروفسكايتية .(PSCs) تم توصيف جسيمات TiO_2 المُصنَّعة باستخدام تقنيات مطيافية الأشعة تحت الحمراء بتحويل فوريه(FTIR) ، وحيود الأشعة السينية(XRD) ، ومطيافية الانعكاس المنتشر للأشعة فوق البنفسجية–المرئية(UV-Vis DRS) ، والمجهر الإلكتروني الماسح بانبعاث الحقل المزود بتحليل تشتت الطاقة للأشعة السينية(FESEM/EDX) . أكدت نتائج XRD وجود طور الأناتاز النقي مع حجم بلوري أصغر مقارنةً بـ TiO_2 التجاري، بينما أثبت تحليل EDX نجاح التخليق من خلال التحليل العنصري. وأظهرت صور FESEM مزيجاً من الجسيمات الخشنة والمتوزّعة بشكل متجانس. وكشفت الدراسات البصرية عن انخفاض في طاقة فجوة الحزمة (3.0400 eV) مقارنةً بـ TiO_2 التجاري(3.2000 eV) ، مما يشير إلى تحسين القدرة على امتصاص الضوء. تشير النتائج إلى أن دمج GO أسهم بشكل ملحوظ في تعزيز الأداء الكهروضوئي؛ حيث تم تسجيل أعلى كفاءة تحويل للطاقة (0.2467%) في العينة التي تم تخليقها باستخدام الماء المقطر ومستخلص الأوراق و—GOوهي أعلى بمقدار مرتبة كاملة من TiO_2 التجاري (0.0259%). ومع ذلك، اختلف الأداء بشكل واضح تبعاً لوسيط التخليق، مما يدل على أن التفاعلات الخاصة بالمذيب تلعب دوراً حاسماً في تحديد كفاءة الجهاز. تُظهر هذه النتائج إمكانية الاعتماد على التخليق الصديق للبيئة في تطوير المواد النانوية الوظيفية، وتبرز الفوائد التآزرية للجمع بين المُختزلات النباتية وتطعيم GO. كما يوفّر هذا النهج مساراً واعداً نحو تقنيات خلايا بيروفسكايتية أكثر استدامة وأقل تكلفة، رغم أن تحسين تركيب المستخلص النباتي وضبط مورفولوجيا الجسيمات النانوية يظل أمراً أساسياً.

الكلمات المفتاحية: Basella rubra، أكسيد الغرافين، التخليق الأخضر، السبانخ المالاباري، جسيمات ثاني أكسيد التيتانيوم النانوية.